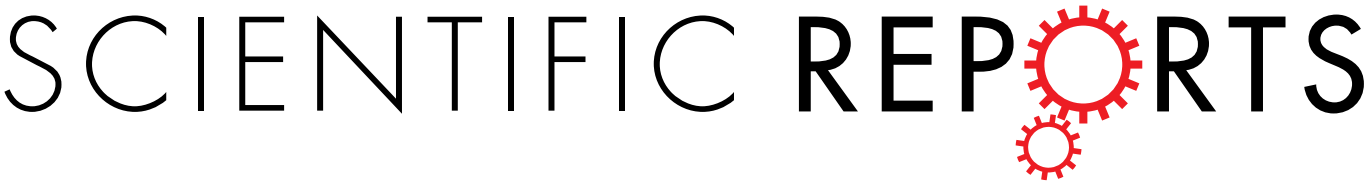

OPEN

Element substitution of kesterite Cu_2ZnSnS_4 for efficient counter electrode of dye-sensitized solar cells

Received: 5 March 2018
Accepted: 14 May 2018
Published online: 07 June 2018

Shuang Lu, Huanying Yang, Fei Li, Yinglin Wang, Shixin Chen, Guochun Yang, Yichun Liu & Xintong Zhang

Development of cost-effective counter electrode (CE) materials is a key issue for practical applications of photoelectrochemical solar energy conversion. Kesterite Cu_2ZnSnS_4 (CZTS) has been recognized as a potential CE material, but its electrocatalytic activity is still insufficient for the recovery of I^-/I_3^- electrolyte in dye-sensitized solar cells (DSSCs). Herein, we attempt to enhance the electrocatalytic activity of kesterite CZTS through element substitution of Zn^{2+} by Co^{2+} and Ni^{2+} cations, considering their high catalytic activity, as well as their similar atomic radius and electron configuration with Zn^{2+}. The Cu_2CoSnS_4 (CCTS) and Cu_2NiSnS_4 (CNTS) CEs exhibit smaller charge-transfer resistance and reasonable power conversion efficiency (PCE) (CCTS, 8.3%; CNTS, 8.2%), comparable to that of Pt (8.3%). In contrast, the CZTS-based DSSCs only generate a PCE of 7.9%. Density functional theory calculation indicate that the enhanced catalytic performance is associated to the adsorption and desorption energy of iodine atom on the Co^{2+} and Ni^{2+}. In addition, the stability of CCTS and CNTS CEs toward electrolyte is also significantly improved as evidenced by X-ray photoelectron spectroscopy and electrochemical impedance spectroscopy characterizations. These results thus suggest the effectiveness of the element substitution strategy for developing high-performance CE from the developed materials, particularly for multicomponent compounds.

High-efficiency, good-stability and low-cost counter electrodes (CEs) are essential for photoelectrochemical solar energy conversion. As a key component of the photoelectrochemical solar cells, the CEs need to possess good conductivity and high catalytic activity for the efficient recovery of redox. Up to now, Pt is the most widely applied CE active materials for dye-sensitized solar cells (DSSCs)[1,2]. However, the high cost of Pt-based materials limits their further development. Numerous candidates are exploited to replace the expensive Pt, such as metals and alloys[3], carbon materials[4,5], conductive polymer[6,7], transition metal compounds[8–10] and composites[11,12]. Among them, the transition metal compounds (TMCs) attract much attention because of their Pt-like catalytic activity[13–19]. Various binary TMC CEs are wildly investigated, however the study of multicomponent TMC CEs is still limited despite they have many advantages, such as material diversity and multiple activity sites[19].

Recently, kesterite Cu_2ZnSnS_4 (CZTS), a quaternary transition metal sulfide, is considered to be a promising photo- and electro-catalyst due to its tunable band gap (1.0–1.5 eV), high abundance and nontoxicity[20–29]. After optimizing composition and morphology of CZTS CE, the efficiency of DSSCs was reported in the range from ~4% to 9%. But, the catalytic activity of CZTS is still limited, due to its fully-filled d orbitals of metallic active sites (Zn^{2+} and Sn^{4+})[30]. Thus, it is reasonable to suppose that the substitution of Zn^{2+} or Sn^{4+} by more active metal ions would enhance the activity of CZTS CE. Co^{2+} and Ni^{2+} are high-activity catalytic sites in various photo- and electro-catalysts[31–38]. Series of highly efficient CE materials based on Co^{2+} and Ni^{2+} have been exploited, including carbides[39], nitrides[40], chalcogenides[41,42] and oxides[43]. Furthermore, these two divalent metal ions present similar atomic radius and electron configuration with Zn^{2+}, thus substituting Zn^{2+} by Co^{2+} or Ni^{2+} may improve the catalytic activity of CZTS.

Center for Advanced Optoelectronic Functional Materials Research, and Key Lab of UV-Emitting Materials and Technology of Ministry of Education, Northeast Normal University, 5268 Renmin Street, Changchun, 130024, China. Correspondence and requests for materials should be addressed to Y.W. (email: wangyl100@nenu.edu.cn) or X.Z. (email: xtzhang@nenu.edu.cn)

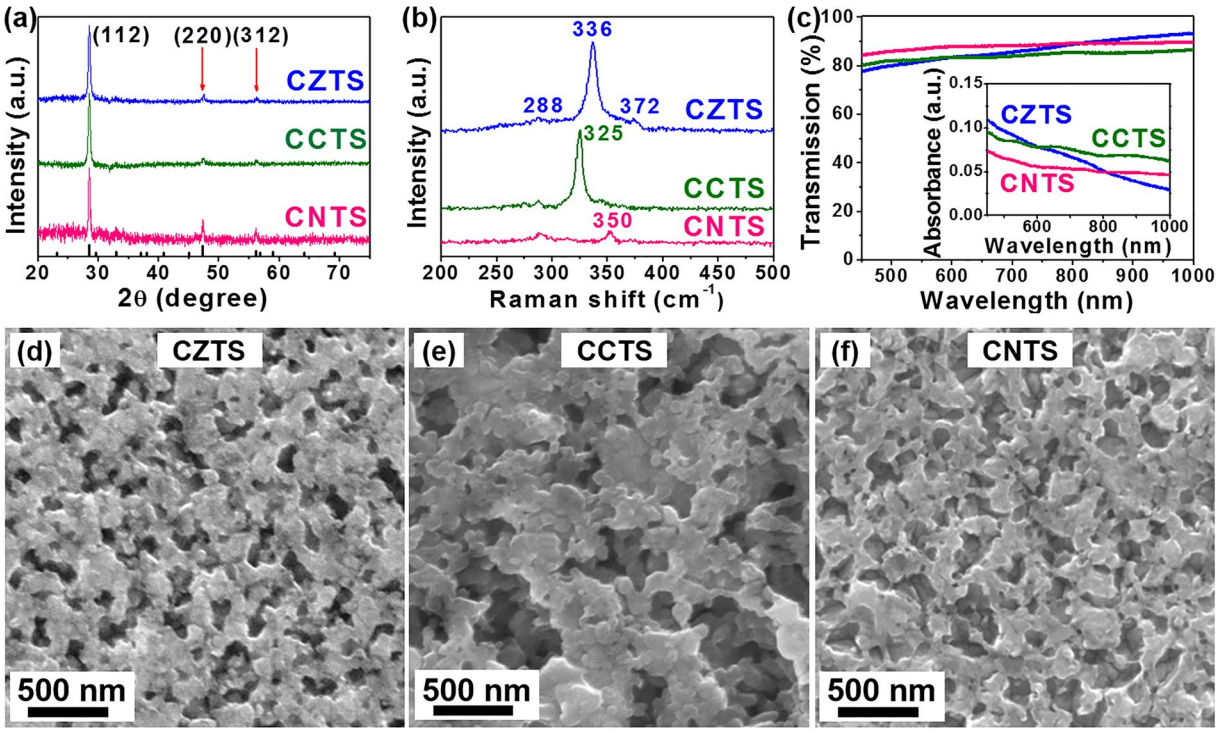

Figure 1. (**a**–**c**) XRD patterns, Raman and UV-Vis spectra and (**d**–**f**) top-view SEM images of CXTS films prepared by H_2O/ethanol precursor solutions. The films of XRD and Raman measurements were prepared on quartz.

Herein, we investigate the effect of element substitution on improving the electrocatalytic activity of kesterite CZTS CEs. We prepare kesterite Cu_2XSnS_4 (X = Zn, Co, Ni) CEs by simple spin-coating method. Electrochemical impedance spectroscopy (EIS) and X-ray photoelectron spectroscopy (XPS) tests indicate that the Cu_2CoSnS_4 (CCTS) and Cu_2NiSnS_4 (CNTS) CEs possess decreased change-transfer resistance and improved stability toward iodide electrolyte. CCTS- and CNTS-based DSSCs exhibit enhanced efficiency (8.3% and 8.2%) compared with that of CZTS (7.9%), which is comparable with traditional Pt (8.3%). In addition, the highly-effective catalytic activity is related to the adsorption and desorption energy of iodine (I) atom calculated by the density functional theory[44–47].

Results and Discussion

Structure and morphology characterizations. We prepared porous CXTS films by spin-coating precursor solutions based on water and ethanol mixed solvent and annealing them in N_2 atmosphere at 540 °C for 15 minutes[48]. To avoid the signals interference of FTO (SnO_2: F) to CXTS films, we recorded X-ray diffraction (XRD) patterns and Raman spectra through CXTS films on quartz prepared by the same method. The diffraction peaks at 28.53°, 47.33°, and 56.18° were indexed to (112), (220), and (312) planes respectively, which were in good agreement with those of previously reported kesterite CZTS[48–50] (Fig. 1(a)). This measurement indicated that the element substitution did not change the crystal structure of CZTS. Furthermore, three peaks at 288, 336 and 372 cm^{-1} were observed in the Raman spectra (Fig. 1(b)) of CZTS, which were indexed to CZTS materials. The CCTS and CNTS spectra showed peaks at 288, 325 and 350 cm^{-1}, which were observed in the CCTS and CNTS materials of previous literatures[51–54]. In addition, we used Energy-dispersive X-ray spectroscopy (EDX) to analyze the composition of CXTS films (Fig. S1(a–c) in the Supplementary Information). The elemental composition ratio was 1.8:1:1.3:4.7, 1.5:1:1.3:4.4 and 1.5:1:1.1:4, respectively. These results indicated that the CXTS CEs was successfully synthesized. In addition, CXTS CEs showed above 75% transmittance in the range of visible wavelengths as shown in the UV-Vis spectra of Fig. 1(c).

Figure 1(d–f) exhibited the top-view scanning electron microscope (SEM) images of the CXTS films. It was obvious that the CXTS films showed a porous structure, which was beneficial to the high catalytic activity because of the high specific surface area[55]. The Atomic force microscope (AFM) measurements also showed similar morphology (see Fig. S1(d–f) in the Supplementary Information). We performed step profiler test to accurately measure the thickness of CXTS films. The thickness of CZTS, CCTS and CNTS CEs were calculated to be 189 ± 13 nm, 125 ± 3 nm and 148 ± 27 nm, respectively, from nine measure points. The thickness of CXTS films was carefully optimized by spin-coating 1 layer of precursor solution (see Fig. S2 in the Supplementary Information) providing enough active sites and reduced bulk resistance.

Electrochemical characterization. To investigate the electrocatalytic activity of kesterite CXTS CEs for reducing iodide electrolyte, we performed Tafel polarization measurements with the symmetrical structure (CE//

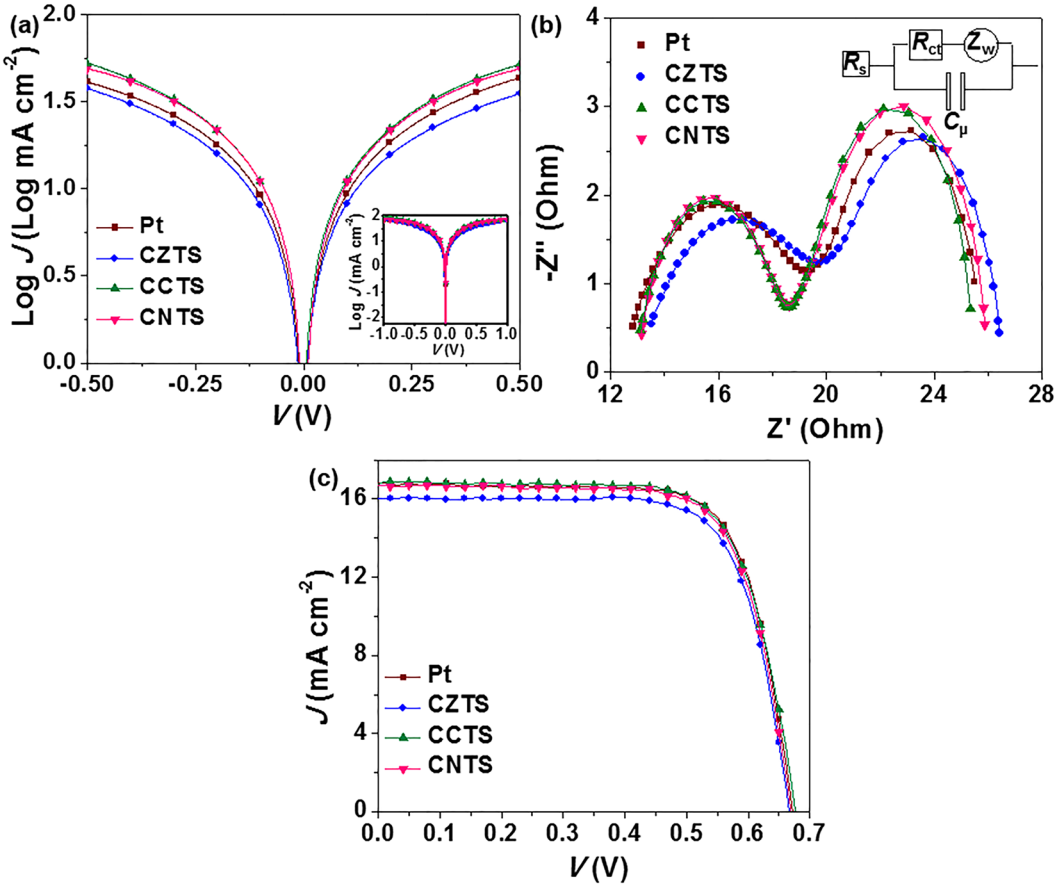

Figure 2. (**a**) Tafel curves and (**b**) EIS plots of Pt and CXTS CEs. Both Tafel and EIS experiments were performed with the symmetrical dummy cells with two identical electrodes (CE//iodide electrolyte//CE). Inset in a and b show the original Tafel curves and the equivalent circuit model of the symmetrical cells for fitting EIS results. (**c**) *J*–*V* curves of DSSCs based on Pt and CXTS CEs, measured under AM 1.5 G solar simulator illumination (100 mW cm^{-2}).

electrolyte//CE). The exchange current density (J_0) of CEs could be acquired from the intercept of a tangent to Tafel polarization curves (Tafel), the variation of which could be inverse with the charge-transfer resistance (R_{ct}) values fitted from EIS through eq. 1:

$$J_0 = \frac{RT}{nFR_{ct}} \quad (1)$$

where R is the gas constant, T is the temperature, F is Faraday's constant and n is the electron number involved in the electrochemical reduction of triiodides at the electrode[56]. As shown in Fig. 2(a), the anodic and cathodic branches of CCTS- and CNTS-Tafel curves exhibited larger slopes than those of CZTS, revealing a higher J_0 and more efficient catalytic activity of CCTS and CNTS CEs for reducing triiodides. In addition, we also prepared Cu_2MnSnS_4 and Cu_2FeSnS_4 CEs by similar method. However, their performance was poor because of the bad activity and unstable chemical property of these two films.

The EIS test was used to further evaluate the catalytic activity of CXTS CEs. The left arcs of EIS spectra in Fig. 2(b) reflects the R_{ct} and series resistance (R_s) whose exact values are obtained by fitting the equivalent circuit in the inset of Fig. 2(b). As shown in Table 1, the R_{ct} values were reduced after substituting Zn^{2+} by Co^{2+} and Ni^{2+} ions (CCTS, 5.3 Ω; CNTS, 5.5 Ω; CZTS, 6.5 Ω), which was consistent with the variation of J_0 values in Fig. 2(a). In addition, the R_s values of CCTS and CNTS CEs were close to that of CZTS, indicated their similar electron transport ability. Thus, the variation of R_{ct} led to the enhancement of the catalytic activity of CCTS and CNTS CEs, compared with CZTS. This catalytic activity trend was also observed on dense CXTS films prepared by spin-coating the dimethyl sulphoxide-based precursor solution (see Fig. S3 in the Supplementary Information). All the electrochemical data suggested that the substitution of Zn^{2+} by Co^{2+} and Ni^{2+} effectively improved the electrocatalytic activity of kesterite CZTS CEs for reducing triiodides.

Photovoltaic performance of DSSCs. The current density-voltage (*J*–*V*) curves of DSSCs containing Pt or CXTS CEs and N719-sensitized TiO_2 photoanode in iodide electrolyte were shown in Fig. 2(c). Table 1 summarizes the resultant photovoltaic parameters. The CCTS- and CNTS-based DSSCs revealed comparable power

CE	R_s (Ω)	R_{ct} (Ω)	J_{sc} (mA cm^{-2})	V_{oc} (V)	FF	PCE (%)
Pt	12.4	5.9	16.80	0.68	0.73	8.3
CZTS	13.1	6.5	16.05	0.67	0.73	7.9
CCTS	12.9	5.3	16.79	0.68	0.72	8.3
CNTS	12.9	5.5	16.74	0.67	0.73	8.2

Table 1. Electrochemical parameters of EIS plots with Pt and CXTS CEs and photovoltaic parameters obtained from DSSCs with Pt and CXTS CEs.

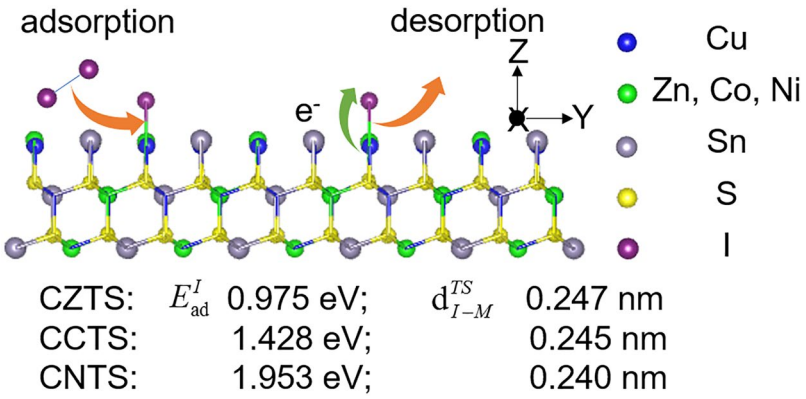

Figure 3. The schematic diagram of reducing triiodides on CXTS (112) surface: adsorption of I_2, electron transfer, desorption of I^*. The corresponding adsorption energy E^I_{ad}, bond length d^{TS}_{I-M} are also shown.

conversion efficiency (PCE) (8.3% and 8.2%, respectively) with that of Pt-based DSSC (8.3%), which were derived from the short-circuit current density (J_{sc}) of 16.79 and 16.74 mA cm^{-2}, open-circuit voltage (V_{oc}) of 0.68 V and 0.67 V, and fill factor (FF) of 0.72 and 0.73. The CCTS and CNTS cells exhibit a higher J_{sc} and PCE than that of CZTS (J_{sc}, 16.05 mA cm^{-2}; PCE, 7.9%) owing to the higher activity of the CCTS and CNTS CEs. In addition, photovoltaic parameters of five parallel CXTS-based DSSCs indicate the good repeatability of CXTS CEs (see Fig. S4 and Table S1 in the Supplementary Information). Therefore, the electrochemical data of dummy cells and photovoltaic performance of DSSCs confirm that substitution of Zn^{2+} by Co^{2+} and Ni^{2+} is effective for improving the electrocatalytic ability of kesterite CZTS CEs.

Density functional theory calculation. Considering that the catalytic activity of CEs strongly correlates with the adsorption and desorption processes of redox species, we perform density functional theory calculation to explore the origin of catalysis-activity enhancement caused by element substitution. First, we checked the change of adsorption energy toward I atom (E^I_{ad}) during the substitution of Zn^{2+} by Co^{2+} and Ni^{2+}. We found that the I atom was preferentially adsorbed on Zn^{2+} of CZTS, as the calculated E^I_{ad} value of Sn^{4+} (0.295 eV) was significantly lower than that of Zn^{2+} (0.975 eV) (see Fig. S5 in the Supplementary Information). And the E^I_{ad} value (Fig. 3 and Fig. S5 in the Supplementary Information) remarkably increased to 1.428 eV (CCTS) and 1.953 eV (CNTS) after the element substitution. This change indicated the stronger adsorption ability toward I atom of CCTS and CNTS CEs, resulted in their more efficient catalytic activity for reducing triiodides. Moreover, the calculated bond length between I atom and metal ions for the transition state (d^{TS}_{I-M}) decreased from 0.247 nm of CZTS to 0.245 nm of CCTS and 0.240 nm of CNTS, which could result in more difficult desorption of the adsorbed I atom (I^*). These theoretical calculation data showed that the enhanced performance of CCTS and CNTS CEs compared CZTS was associated to the improved adsorption and desorption energy.

Furthermore, we compared the amounts of I atom adsorbed on the CXTS surface by XPS[57–60] (see Fig. S6 in the Supplementary Information and Fig. 4). We immersed CXTS CEs in the iodide electrolyte for 30 minutes and rinsed them with ethanol. The peak area ratio of I 3d to Cu 2p spectra was marked as the normalized peak area of I 3d spectra. No signals of I 3d were found in XPS results before immersing. But, after immersing, the normalized peak area of I 3d spectra of CCTS (0.1894) and CNTS (0.1621) were significantly larger than that of CZTS (0.0443) (Fig. 4(b)), indicating more I atom adsorbed on CCTS and CNTS CEs surface. This change was consistent with the enhanced E^I_{ad} values and decreased bond length. The electrochemical, photovoltaic and theoretical results all indicated that the substitution of Zn^{2+} by Co^{2+} and Ni^{2+} was effective to improve the catalytic activity of kesterite CZTS.

Durability test. The stability is one of the major factors to evaluate the property of CEs[61–63]. Herein, we used Tafel, EIS and XPS tests to examine the stability of CXTS CEs. First, the current density in Tafel curves at −0.40 V (see Fig. S7 in the Supplementary Information) of the CZTS CEs decreased by 6% compared with the original ones after 1800 s test (Fig. 5). Whereas, the current density of Pt, CCTS and CNTS CEs only decreased by less than 3%, indicating the better stability of CCTS and CNTS CEs. The fitted R_s and R_{ct} values obtained from EIS

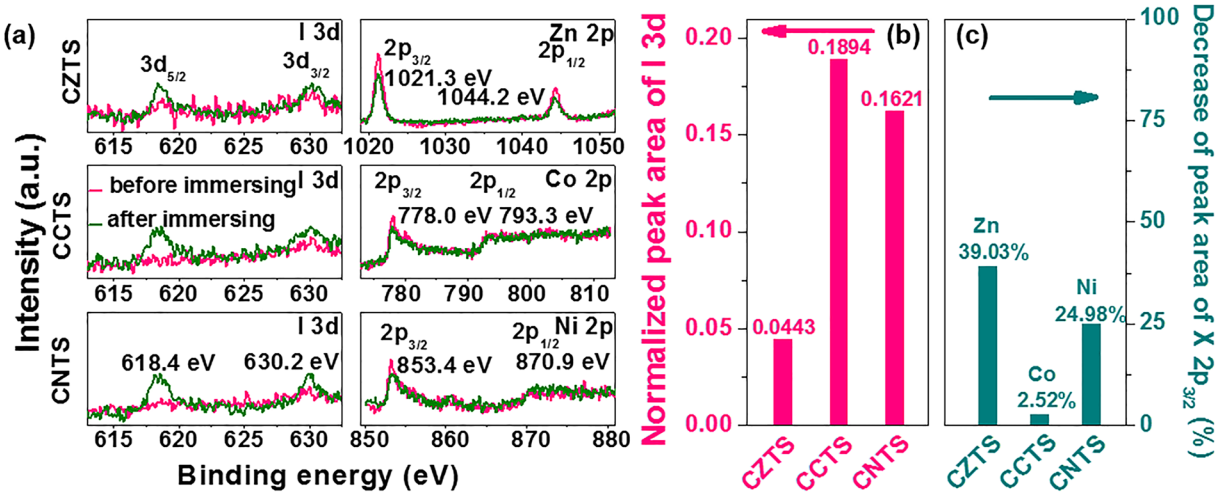

Figure 4. (**a**) I 3d, Zn 2p, Co 2p and Ni 2p XPS spectra of CXTS CEs before and after immersing in the iodide electrolyte for 30 minutes. (**b**) The normalized peak area of I 3d XPS spectra of CXTS CEs after immersing in the iodide electrolyte for 30 minutes and (**c**) the decrease of peak area of X $2p_{3/2}$ XPS spectra of CXTS CEs after immersing.

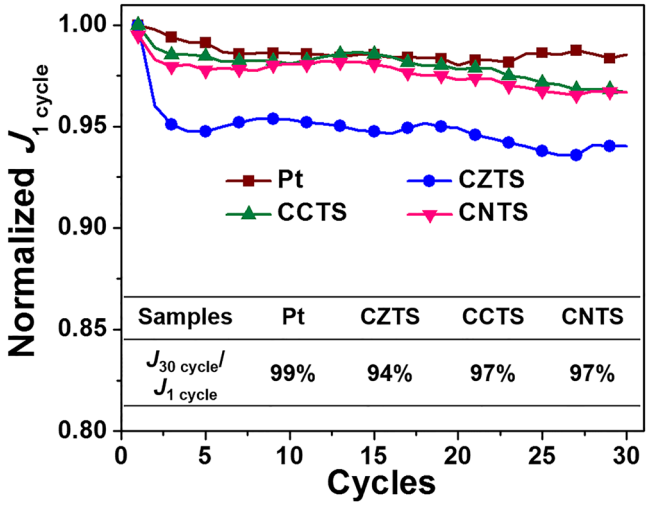

Figure 5. The change of the current density under −0.40 V for different cycles of Tafel polarization measurement of Pt and CXTS CEs. The current density of the first cycle and the last cycle are marked as J_1 cycle and J_{30} cycle, respectively.

spectra of CXTS CEs before and after immersing in the iodide electrolyte for 30 minutes (see Fig. S8 and Table S2 in the Supplementary Information) also showed the good stability of CCTS and CNTS. In addition, after immersing, the peak area of Co and Ni XPS spectra decreased by 2.52% and 24.98% of the original ones, respectively (Fig. 4(c)). This result was significantly smaller than that of Zn spectra in CZTS (39.03%). Different stability measurements all suggested that the CCTS and CNTS CEs possessed better stability toward the iodide electrolyte compared with CZTS CE.

Conclusions

In conclusion, we proved that the substitution of Zn^{2+} by Co^{2+} and Ni^{2+} was a convenient but effective approach to enhance the electrocatalytic performance of kesterite CZTS CEs in DSSCs. After substitution, CCTS and CNTS CEs exhibited decreased charge transfer resistance (CCTS, 5.3 Ω; CNTS, 5.5 Ω; CZTS, 6.5 Ω) and improved electrocatalytic activity (PCE: CCTS, 8.3%; CNTS, 8.2%) compared with CZTS (7.9%) toward iodide electrolyte, which was comparable with the traditional Pt-based cells (8.3%). The enhanced activity was associated to the change of adsorption and desorption energy (the bond length between I atom and metal ions for the transition state (d^{TS}_{I-M}) of I atom by theoretical calculation. Furthermore, the stability of kesterite CXTS CEs was also significantly improved. The results indicated that this element substitution method without changing the materials

structure was effective to improve potential catalysts performance, especially for the multicomponent compounds.

References

1. Thomas, S. *et al*. A review on counter electrode materials in dye-sensitized solar cells. *J. Mater. Chem. A* **2**, 4474–4490 (2014).
2. Kakiage, K. *et al*. Fabrication of a high-performance dye-sensitized solar cell with 12.8% conversion efficiency using organic silyl-anchor dyes. *Chem. Commun.* **51**, 6315–6317 (2015).
3. Huang, S. *et al*. Improving the catalytic performance of Ni_3S_4-PtCo heteronanorods via Mott-Schottky effect toward the reduction of iodine couples in dye-sensitized solar cells. *Electrochim. Acta* **241**, 89–97 (2017).
4. Bora, A., Mohan, K., Phukan, P. & Dolui, S. A low cost carbon black/polyaniline nanotube composite as efficient electro-catalyst for triiodide reduction in dye sensitized solar cells. *Electrochim. Acta* **259**, 233–244 (2018).
5. Pazoki, M., Cappel, U., Johansson, E., Hagfeldt, A. & Boschloo, G. Characterization techniques for dye-sensitized solar cells. *Energy Environ. Sci.* **10**, 672–709 (2017).
6. Zhang, X. *et al*. Synthesis of Wurtzite Cu_2ZnSnS_4 Nanosheets with Exposed High-Energy (002) Facets for Fabrication of Efficient Pt-Free Solar Cell Counter Electrodes. *Scientific Reports* **8**, 248 (2018).
7. Yun, S. *et al*. Dye-sensitized solar cells employing polymers. *Prog. Polym. Sci.* **59**, 1–40 (2016).
8. Liu, X., Gao, L., Yue, G., Zheng, H. & Zhang, W. Efficient dye-sensitized solar cells incorporating hybrid counter electrode of $CuMnSnS_4$ microsperes/carbon nanotubes. *Sol. Energy* **158**, 952–959 (2017).
9. Wang, X. *et al*. Selenization of Cu_2ZnSnS_4 Enhanced the Performance of Dye-Sensitized Solar Cells: Improved Zinc-Site Catalytic Activity for I_3^-. *ACS Appl. Mater. Interfaces* **9**, 37662–37670 (2017).
10. Zhang, X. *et al*. Significant Broadband Photocurrent Enhancement by Au-CZTS Core-Shell Nanostructured Photocathodes. *Scientific Reports* **6**, 23364 (2016).
11. Li, L. *et al*. Preparation of carbon nanofibers supported MoO_2 composites electrode materials for application in dye-sensitized solar cells. *Electrochim. Acta* **259**, 188–195 (2018).
12. Yun, S., Hagfeldt, A. & Ma, T. Superior Catalytic Activity of Sub-5 mm-Thick Pt/SiC Films as Counter Electrodes for Dye-Sensitized Solar Cells. *Chem Cat Chem* **6**, 1584–1588 (2014).
13. Hao, F. *et al*. Recent advances in alternative cathode materials for iodine-free dye-sensitized solar cells. *Energy Environ. Sci.* **6**, 2003–2019 (2013).
14. Hussain, S. *et al*. Large area growth of $MoTe_2$ films as high performance counter electrodes for dye-sensitized solar cells. *Scientific Reports* **8**, 29 (2018).
15. Muralee Gopi, C., Ravi, S., Rao, S., Reddy, A. & Kim, H. Carbon nanotube/metal-sulfde composite flexible electrodes for high-performance quantum dot-sensitized solar cells and supercapacitor. *Scientific Reports* **9**, 46519 (2017).
16. Ye, M. *et al*. Recent advances in dye-sensitized solar cells: from photoanodes, sensitizers and electrolytes to counter electrodes. *Mater. Today* **18**, 155–162 (2015).
17. Liu, F. *et al*. Low-temperature, solution-deposited metal chalcogenide films as highly efficient counter electrodes for sensitized solar cells. *J. Mater. Chem. A* **3**, 6315–6323 (2015).
18. Singh, E., Kim, K., Yeom, G. & Nalwa, H. Two-dimensional transition metal dichalcogenide based counter electrodes for dye-sensitized solar cells. *RSC Adv.* **7**, 28234–28249 (2017).
19. Wu, J. *et al*. Counter electrodes in dye-sensitized solar cells. *Chem. Soc. Rev.* **46**, 5975–6023 (2017).
20. Woo, K., Kim, Y. & Moon, J. A non-toxic, solution-processed, earth abundant absorbing layer for thin-film solar cells. *Energy Environ. Sci.* **5**, 5340–5345 (2012).
21. Chiu, J. *et al*. Geogrid-Inspired Nanostructure to Reinforce a $Cu_xZn_ySn_zS$ Nanowall Electrode for High-Stability Electrochemical Energy Conversion Devices. *Adv. Energy Mater.* **7**, 1602210 (2017).
22. Chen, H., Wang, J., Jia, C., Mou, J. & Zhu, L. Highly efficient dye-sensitized solar cell with a novel nanohybrid film of Cu_2ZnSnS_4-MWCNTs as counter electrode. *Appl. Surf. Sci.* **422**, 591–596 (2017).
23. Pang, Z. *et al*. Direct growth of Cu_2ZnSnS_4 on three-dimensional porous reduced graphene oxide thin films as counter electrode with high conductivity and excellent catalytic activity for dye-sensitized solar cells. *J. Mater. Sci.* **53**, 2748–2757 (2018).
24. Swami, S., Chaturvedi, N., Kumar, A. & Dutta, V. Dye sensitized solar cells using the electric field assisted spray deposited kesterite (Cu_2ZnSnS_4) films as the counter electrodes for improved performance. *Electrochim. Acta* **263**, 26–33 (2018).
25. Özel, F. *et al*. Penternary chalcogenides nanocrystals as catalytic materials for efficient counter electrodes in dye-synthesized solar cells. *Scientific Reports* **6**, 29207 (2016).
26. Xin, X., He, M., Han, W., Jung, J. & Lin, Z. Low-Cost Copper Zinc Tin Sulfide Counter Electrodes for High-Efficiency Dye-Sensitized Solar Cells. *Angew. Chem. Int. Ed.* **50**, 11739–11742 (2011).
27. Chen, S. *et al*. *In situ* synthesis of two-dimensional leaf-like Cu_2ZnSnS_4 plate arrays as a Pt-free counter electrode for efficient dye-sensitized solar cells. *Green Chem.* **18**, 2793–2801 (2016).
28. Hou, Z. *et al*. Magnetron sputtering route to efficiency enhanced Cu_2ZnSnS_4 thin films as the counter electrode of dye-sensitized solar cells. *Sci. Adv. Mater.* **5**, 1764–1769 (2013).
29. Fan, M., Chen, J., Li, C., Cheng, K. & Ho, K. Copper zinc tin sulfide as a catalytic material for counter electrodes in dye-sensitized solar cells. *J. Mater. Chem. A* **3**, 562–569 (2015).
30. Yu, X. *et al*. Cu_2ZnSnS_4 Nanocrystals as Highly Active and Stable Electrocatalysts for the Oxygen Reduction Reaction. *J. Phys. Chem. C* **120**, 24265–24270 (2016).
31. Sharma, V., Singh, I. & Chandra, A. Hollow nanostructures of metal oxides as next generation electrode materials for supercapacitors. *Scientific Reports* **8**, 1307 (2018).
32. Wu, Y. *et al*. The nanoscale effects on the morphology, microstructure and electrochemical performances of the cathodic deposited α-$Ni(OH)_2$. *Electrochim. Acta* **261**, 58–65 (2018).
33. Ao, K. *et al*. Fe-doped Co_9S_8 nanosheets on carbon fiber cloth as pH-universal freestanding electrocatalysts for efficient hydrogen evolution. *Electrochim. Acta* **264**, 157–165 (2018).
34. Ma, Z. *et al*. Three-dimensional well-mixed/highly-densed NiS-CoS nanorod arrays: An efficient and stable bifunctional electrocatalyst for hydrogen and oxygen evolution reactions. *Electrochim. Acta* **260**, 82–91 (2018).
35. Kim, D. *et al*. Chemical synthesis of hierarchical $NiCo_2S_4$ nanosheets like nanostructure on fexible foil for a high performance supercapacitor. *Scientific Reports* **7**, 9764 (2017).
36. Jin, Z., Zhang, M., Wang, M., Feng, C. & Wang, Z. Metal Selenides as Efficient Counter Electrodes for Dye-Sensitized Solar Cells. *Acc. Chem. Res.* **50**, 895–904 (2017).
37. Liu, Y. *et al*. Coupling Sub-Nanometric Copper Clusters with Quasi-Amorphous Cobalt Sulfide Yields Efficient and Robust Electrocatalysts for Water Splitting Reaction. *Adv. Mater.* **29**, 1606200 (2017).
38. Lu, S. *et al*. Adsorption Energy Optimization of Co_3O_4 through Rapid Surface Sulfurization for Efficient Counter Electrode in Dye-Sensitized Solar Cells. *J. Phys. Chem. C* **121**, 12524–12530 (2017).
39. Yun, S. *et al*. Metal Oxide/Carbide/Carbon Nanocomposites: *In Situ* Synthesis, Characterization, Calculation, and their Application as an Efficient Counter Electrode Catalyst for Dye-Sensitized Solar Cells. *Adv. Energy Mater.* **3**, 1407 (2013).

40. Wu, M. *et al*. Economical Pt-Free Catalysts for Counter Electrodes of Dye Sensitized Solar Cells. *J. Am. Chem. Soc.* **134**, 3419–3428 (2012).
41. Sun, H., Wang, G. & Wang, Z. Co_9Se_8 Nanosheets Electrodes: Drop-Cast versus *in situ* Growth. *Chinese J. Chem.* **35**, 645–650 (2017).
42. Jia, J. *et al*. Influence of deposition voltage of cobalt diselenide preparation on the film quality and the performance of dye-sensitized solar cells. *Sol. Energy* **151**, 61–67 (2017).
43. Yun, S., Hagfeldt, A. & Ma, T. Pt-Free Counter Electrode for Dye-Sensitized Solar Cells with High Efficiency. *Adv. Mater.* **26**, 6210–6237 (2014).
44. Hou, Y. *et al*. Rational screening low-cost counter electrodes for dye-sensitized solar cells. *Nat. Commun.* **4**, 1583 (2013).
45. Wang, D., Jiang, J., Wang, H. & Hu, P. Revealing the Volcano-Shaped Activity Trend of Triiodide Reduction Reaction: A DFT Study Coupled with Microkinetic Analysis. *ACS Catal.* **6**, 733–741 (2016).
46. Zhang, B. *et al*. Facet-dependent catalytic activity of platinum nanocrystals for triiodide reduction in dye-sensitized solar cells. *Scientific Reports* **3**, 1836 (2013).
47. Chen, J., Mao, Y., Wang, H. & Hu, P. Theoretical study of heteroatom doping in tuning the catalytic activity of graphene for triiodide reduction. *ACS Catal.* **6**, 6804–6813 (2016).
48. Xiao, Z. *et al*. Significantly enhancing the stability of a Cu_2ZnSnS_4 aqueous/ethanol-based precursor solution and its application in $Cu_2ZnSn(S,Se)_4$ solar cells. *RSC Adv.* **5**, 103451–103457 (2015).
49. Liu, F. *et al*. Kesterite Cu_2ZnSnS_4 thin film solar cells by a facile DMF-based solution coating process. *J. Mater. Chem. C* **3**, 10783–10792 (2015).
50. Mali, S., Patil, P. & Hong, C. Low-Cost Electrospun Highly Crystalline Kesterite Cu_2ZnSnS_4 Nanofiber Counter Electrodes for Efficient Dye-Sensitized Solar Cells. *ACS Appl. Mater. Interfaces* **6**, 1688–1696 (2014).
51. Mokurala, K., Mallick, S. & Bhargava, P. Alternative quaternary chalcopyrite sulfides (Cu_2FeSnS_4 and Cu_2CoSnS_4) as electrocatalyst materials for counter electrodes in dye-sensitized solar cells. *J. Power Sources* **305**, 134–143 (2016).
52. Benchikri, M. *et al*. A high temperature route to the formation of highly pure quaternary chalcogenide particles. *Mater. Lett.* **68**, 340–343 (2012).
53. Chen, H., Fu, S., Tsai, T. & Shih, C. Quaternary Cu_2NiSnS_4 thin films as a solar material prepared through electrodeposition. *Mater. Lett.* **166**, 215–218 (2016).
54. Podsiadlo, S. *et al*. Synthesis of magnetic doped kesterite single crystals. *Cryst. Res. Technol.* **50**, 690–694 (2015).
55. Vanrenterghem, B. *et al*. The reduction of benzylbromide at Ag-Ni deposits prepared by galvanic replacement. *Electrochim. Acta* **196**, 756–768 (2016).
56. Murakami, T. & Grätzel, M. Counter electrodes for DSC: Application of functional materials as catalysts. *Inorg. Chim. Acta* **361**, 572–580 (2008).
57. Xie, Y. *et al*. Highly crystalline stannite-phase Cu_2XSnS_4 (X = Mn, Fe, Co, Ni, Zn and Cd) nanoflower counter electrodes for ZnO-based dye-sensitised solar cells. *J. Alloy. Compd.* **696**, 938–946 (2017).
58. Ramasamy, K., Zhang, X., Bennett, R. & Gupta, A. Synthesis, photoconductivity and self-assembly of wurtzite phase $Cu_2Cd_xZn_{1-2x}SnS_4$ nanorods. *RSC Adv.* **3**, 1186–1193 (2013).
59. Mao, P., Liu, Y., Jiao, Y., Chen, S. & Yang, Y. Enhanced uptake of iodide on $Ag@Cu_2O$ nanoparticles. *Chemosphere* **16**, 396–403 (2016).
60. Li, K. *et al*. Combined DFT and XPS investigation of iodine anions adsorption on the sulfur terminated (001) chalcopyrite surface. *Appl. Surf. Sci.* **390**, 412–421 (2016).
61. Yun, S., Lund, P. & Hinsch, A. Stability assessment of alternative platinum free counter electrodes for dye-sensitized solar cells. *Energy Environ. Sci.* **8**, 3495–3514 (2015).
62. Yun, S., Pu, H., Chen, J., Hagfeldt, A. & Ma, T. Enhanced Performance of Supported HfO_2 Counter Electrodes for Redox Couples Used in Dye-Sensitized Solar Cells. *Chem Sus Chem* **7**, 442–450 (2014).
63. Zhang, C. *et al*. Electrospun FeS nanorods with enhanced stability as counter electrodes for dye-sensitized solar cells. *Electrochim. Acta* **229**, 229–238 (2017).

Acknowledgements

The work was supported by the Natural Science Foundation of China (Grants 51372036, and 51602047) and the Key Project of China Ministry of Education (No. 113020 A). The authors sincerely acknowledge Dr. Hancheng Zhu for providing technology supporting characterization of the samples.

Author Contributions

S. Lu and H. Yang performed the experiments. F. Li and G. Yang performed the theoretical calculations. S. Chen helped to fabricate the samples. S. Lu, Y. Wang, X. Zhang and Y. Liu wrote the manuscript.

Additional Information

Supplementary information accompanies this paper at https://doi.org/10.1038/s41598-018-26770-1.

Competing Interests: The authors declare no competing interests.

Publisher's note: Springer Nature remains neutral with regard to jurisdictional claims in published maps and institutional affiliations.